If the phosphine cluster, $Fe_2Co(CO)_9CPMe_3^-$, is reacted with acid, the H^+ ends up bridging the two Fe atoms, never bonded to the Co. The molecular orbital calculations reveal that the nature of the HOMO of $Fe_2Co(CO)_9CPMe_3^-$ is perfectly suited for this position of attack. The HOMO of $Fe_2Co(CO)_9CPMe_3^-$ is composed of 29% Fe1 and 28% Fe2 orbitals and only 3% Co orbitals. Migration to the carbide, which occurs in $Fe_2Co(CO)_9CCO^-$, is prevented by the superior bonding of the phosphorus atom to the carbide.

Acknowledgment. J.F.O. thanks the IBM Corp. and Southwest Missouri State University for support of this work.

OM920020C

Comparison of the Dynamics and Thermodynamics of the Redox-Promoted Carbonylation of (η-Cp)(CO)(L)FeMe in Methylene Chloride and Acetonitrile. Applications of the Quantitative Analysis of Ligand Effects (QALE)

David C. Woska, Matthew Wilson, Joshua Bartholomew, Klaas Eriks, Alfred Prock,* and Warren P. Giering*

Department of Chemistry, Arthur G. B. Metcalf Center for Science and Engineering, Boston University, Boston, Massachusetts 02215

Received April 21, 1992

The redox-catalyzed carbonylations of 19 complexes, (η-Cp)(CO)(L)FeMe (L = PMe_3, $PPhMe_2$, PEt_3, PPh_2Me, PEt_2Ph, PPh_2Et, P(*i*-Bu)$_3$, P(*p*-$Me_2NC_6H_4$)$_3$, P(*p*-$MeOC_6H_4$)$_3$, P(*p*-MeC_6H_4)$_3$, PPh_3, P(*p*-FC_6H_4)$_3$, P(*p*-ClC_6H_4)$_3$, P(*p*-$CF_3C_6H_4$)$_3$, PPh_2Cy, PPh_2-*t*-Bu, P(*i*-Pr)$_3$, $PPhCy_2$, PCy_3), in acetonitrile have been studied by cyclic and square-wave voltammetry coupled with computer simulation methods. The mechanism appears to involve oxidation of (η-Cp)(CO)(L)FeMe and rapid formation of (η-Cp)(AN)(L)$FeCOMe^+$ followed by rate-limiting reaction of (η-Cp)(AN)(L)$FeCOMe^+$ with CO. Quantitative analysis of the ligand effect data shows that the second-order transformation of (η-Cp)(CO)(L)$FeMe^+$ to (η-Cp)(AN)(L)$FeCOMe^+$ is accelerated by poorer electron donor ligands and inhibited by the larger ligands. The first-order back-reaction of (η-Cp)(AN)(L)$FeCOMe^+$ to (η-Cp)(CO)(L)$FeMe^+$, in contrast, is relatively insensitive to the electron-donor capacity and the size of L. The second-order reaction between (η-Cp)(AN)(L)$FeCOMe^+$ and CO is accelerated by better electron-donor ligands; the steric profile is complex and shows sequential regions of no steric effects, steric acceleration, and steric inhibition. The results of the studies are compared with those obtained when methylene chloride is the solvent.

Introduction

Recently, we reported results of electrochemical studies of the redox-promoted carbonylation of (η-Cp)(CO)(L)-FeMe in methylene chloride containing tetrabutylammonium hexafluorophosphate.[1] The carbonylation proceeds via the iron(III) complexes (η-Cp)(CO)(L)$FeMe^+$ and apparently involves two steps (Scheme I). We suggested that the rate-limiting first step is the nucleophilically (PF_6^- or CH_2Cl_2) assisted alkyl to acyl rearrangement. This result is consisted with the earlier reports of Bergman,[2] Halpern,[3] Cotton,[4] Norton,[5] and Trogler,[6] who pointed out the importance of solvent participation in the alkyl to acyl rearrangement. The nature of the second step, the reaction between the solvent-coordinated acyl complex and CO, could not be probed, unfortunately, since this fast step is kinetically invisible in this medium. Analysis of the kinetic data for alkyl to acyl rearrangement in methylene chloride, as a function of the stereoelectronic properties of the ancillary phosphorus(III) ligands (L), revealed that the transition state for the rearrangement is electron rich compared to the ground state. The reaction is sterically inhibited for complexes containing L with cone angles (θ) <149°. For larger L, the reaction is sterically accelerated. These observations led us to suggest that the transition state possesses a very weakly bonded entering nucleophile (CH_2Cl_2 or PF_6^-) and an extensively formed acyl ligand.

In this paper, we report our study of the carbonylation of (η-Cp)(CO)(L)$FeMe^+$ in acetonitrile (0.1 M TBAH) under 1 atm of CO at 0 °C. Under these conditions the reaction of the solvent-coordinated acyl complex (η-Cp)(AN)(L)$FeCOMe^+$ with CO is rate-limiting, thereby allowing us to study the steps leading to the carbonylation product (η-Cp)(CO)(L)$FeCOMe^+$.

Experimental Section

General Considerations. All manipulations, preparations, and electrochemical experiments were carried out under argon using standard techniques as previously described.[1] Acetonitrile (AN, HPLC grade) was distilled from calcium hydride immediately before use. Mixtures of CO and argon were prepared using Matheson flow meters. The flow meters were calibrated by measuring the volume of pure gases and mixtures of gases that

(1) Prock, A.; Giering, W. P.; Greene, J. E.; Meirowitz, R. E.; Hoffman, S. L.; Woska, D. C.; Wilson, M.; Chang, R.; Chen, J.; Magnuson, R. H.; Eriks, K. *Organometallics* 1991, *10*, 3479–3485.
(2) Wax, M. J.; Bergman, R. G. *J. Am. Chem. Soc.* 1981, *103*, 7028.
(3) Webb, S. L.; Giandomenico, C. M.; Halpern, J. *J. Am. Chem. Soc.* 1986, *108*, 345.
(4) Cotton, J. D.; Markwell, R. D. *J. Organomet. Chem.* 1990, *388*, 123 and references therein.
(5) Martin, B. D.; Warner, K. E.; Norton, J. R. *J. Am. Chem. Soc.* 1986, *108*, 33–39.
(6) Therien, M. J.; Trogler, W. C. *J. Am. Chem. Soc.* 1987, *109*, 5127.
(7) Bartik, T.; Himmler, T.; Schulte, H.-G.; Seevogel, K. *J. Organomet. Chem.* 1984, *272*, 29.
(8) Tolman, C. A. *Chem. Rev.* 1977, *77*, 313.

0276-7333/92/2311-3343$03.00/0

Scheme I

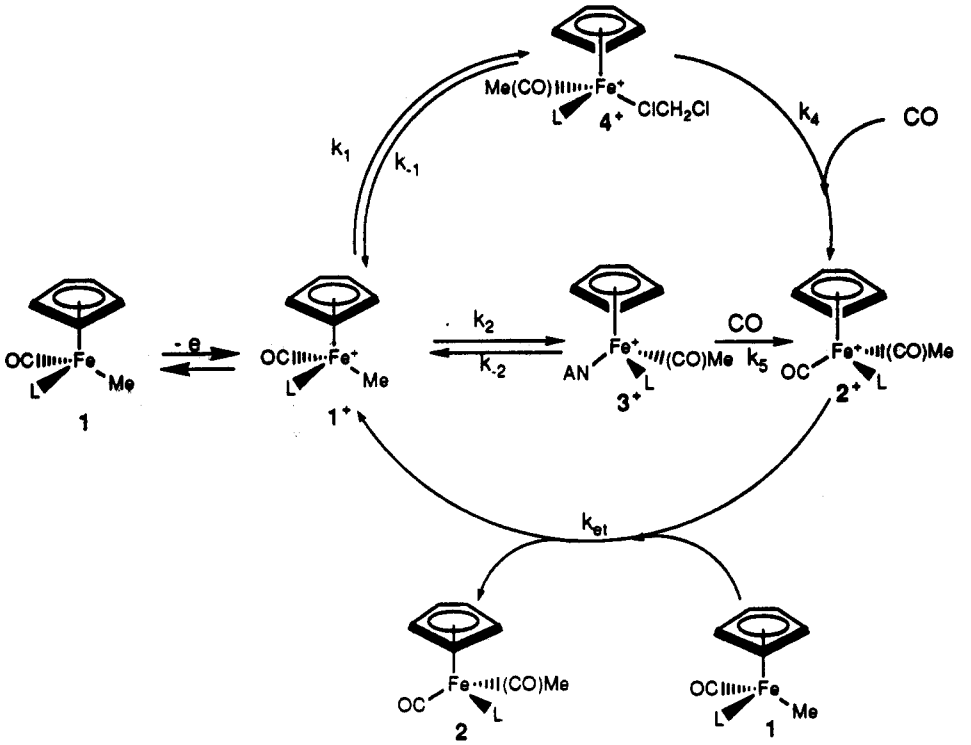

Table I. Stereoelectronic Parameters of Phosphorus(III) Ligands and Rate and Equilibrium Data for the Chemistry Shown in Scheme I

entry no.	L	χ^a	θ^b	$E^{\circ\prime c}$	$K_{eq}{}^d$	$K_{eq}{}^e$	$k_1{}^f$	$k_2{}^{g,h}$	$k_{-2}{}^{h,i}$	$k_5{}^{g,h}$
1	PMe_3	8.55	118	−0.481	65	58	0.068	1.6×10^2	2.4	0.56
2	$PPhMe_2$	10.6	122	−0.443	89	1.1×10^2	0.071	1.6×10^2	1.8	0.30
3	PEt_3	6.3	132	−0.514	5.0	5.8	0.005	13	2.6	1.8
4	$PPhEt_2$	9.3	136	−0.488	11	16	0.041	28	2.5	0.70
5	PPh_2Me	12.2	136	−0.403	1.4×10^2	1.5×10^2	0.059	1.7×10^2	1.3	0.35
6	PPh_2Et	11.3	140	−0.425	55		0.039	68	1.3	1.2
7	$P(i\text{-}Bu)_3$	5.7	143	−0.519	2.0	2.0		6.0	3.0	0.30
8	$P(p\text{-}Me_2NC_6H_4)_3$	5.25	145		1.6	1.2		7.1	4.4	11
9	$P(p\text{-}MeOC_6H_4)_3$	10.5	145	−0.451	54	39	0.042	61	1.6	3.7
10	$P(p\text{-}MeC_6H_4)_3$	11.5	145	−0.430	46	48	0.047	77	1.6	2.8
11	PPh_3	13.25	145	−0.384	1.4×10^2	1.5×10^2	0.067	1.9×10^2	1.4	1.8
12	$P(p\text{-}FC_6H_4)_3$	15.0	145		4.3×10^2	4.3×10^2	0.079	3.8×10^2	0.90	1.3
13	$P(p\text{-}ClC_6H_4)_3$	16.8	145	−0.285	7.1×10^2	5.8×10^2	0.18	4.9×10^2	0.69	0.60
14	$P(p\text{-}F_3CC_6H_4)_3$	20.5	145	−0.205	3.0×10^3	3.4×10^3		1.4×10^3	0.48	
15	PPh_2Cy	9.3	153	−0.457	5.5	7.3	0.02	19	3.4	4.0
16	$PPh_2\text{-}t\text{-}Bu$	8.8	157	−0.480	3.5		0.039	17	4.8	2.4
17	$P(i\text{-}Pr)_3$	3.75	160	−0.581	0.10		0.021	0.80	8.0	8.2
18	$PPhCy_2$	5.35	161	−0.521	0.45		0.027	2.7	6.0	5.1
19	PCy_3	1.4	170	−0.602	0.071		0.024	0.55	7.1	18

[a] Data taken or calculated from data presented in ref 7. [b] Data (deg) calculated or taken from the data presented in ref 8. [c] The reduction potentials (V) for the $1/1^+$ couple were measured relative to the acetylferrocene/acetylferrocenium couple. [d] k_2/k_{-2} (M^{-1}) determined by computer simulation of CV data. [e] Equilibrium constants (M^{-1}) for the interconversion of 1^+ and 3 estimated by the fast-scan cyclic voltammetry method as described in the text. [f] First-order rate constants (s^{-1}). Data taken from ref 1. Data for entries 4, 7, and 16 are reported here for the first time. [g] Second-order rate constants ($M^{-1}\ s^{-1}$). [h] Errors in rate constants are estimated as ±10%. [i] First-order rate constant (s^{-1}).

passed through the meters as a function of time. The concentration of CO in AN was determined to be 7.9 mM by methods previously described.[1]

The kinetic and thermodynamic data were obtained by computer simulation of cyclic voltammetry (CV) and square-wave voltammetry (SWV) data. The simulation method is described in part in a previous paper;[1] below we describe further refinements of this methodology. We then go on to a description of the experiments whose results afford the desired rate constants. The codes for the simulations, which are presented in the supplementary material, are based on the chemistry shown in Scheme I. Rate and equilibrium constants are displayed in Table I.

Simulation of the Electrochemical Experiments. In order to fit electrochemical measurements to a kinetic model, we need the values of electrochemical parameters (heterogeneous rate constants k_h, expressed in terms of the diffusion coefficients D as $k_h\sqrt{D}$, transfer coefficients α, and reduction potentials $E^{\circ\prime}$), as well as homogeneous rate constants for the steps shown in Scheme I. As previously described, we obtained $k_hD^{1/2}$ (an effective value including solution resistance) and α as well as the decomposition rate constants for (η-Cp)(CO)(L)FeMe$^+$ and (η-Cp)(CO)(L)FeCOMe$^+$ from independent CV and SWV measurements in the absence of CO. For these two species (with a given L) the electrochemical parameters prove to be nearly identical. The values of $k_hD^{1/2}$ lie within the range 0.7–5 $s^{-1/2}\ cm^{-1}$. The values of α lie between 0.4 and 0.5. For (η-Cp)(AN)(L)FeCOMe$^+$, which is examined exclusively in CV studies where only its reduction wave is needed, we take $k_hD^{1/2}$ and α to be the same as for (η-Cp)(CO)(L)FeCOMe$^+$. (This assumption is consistent with the observed sweep rate dependence of peak potential in

Table II. Comparison of the Division per Square Wave Cycle (s) and Current Maximum (i_{max}) As Described in the Text

s	40	50	60	80	90	100	110	120
i_{max}	2.1039	2.0853	2.0733	2.0585	2.0536	2.0498	2.0466	2.0440

Table III. Comparison between Simulated and Exact Peak Currents[a]

ΔE_s, mV	E_{sw}, mV	$\Delta\Psi_p$(simulated)	$\Delta\Psi_p$(exact)
5	25	0.5650	0.5649
5	50	0.9185	0.9186
10	50	0.9282	0.9281

[a] See text for definitions of terms.

the reduction of (η-Cp)(AN)(L)FeCOMe$^+$.) The effective reduction potential of (η-Cp)(AN)(L)FeCOMe$^+$ lies about 0.6 V negative of (η-Cp)(CO)(L)FeMe$^+$. A common value of D is employed for all species. Because [CO] was always more than 8 times larger than [(η-Cp)(CO)(L)FeMe], the error introduced for assuming the same D for CO is negligible. Uncertainties are discussed in a previous paper.[1]

Our simulations were done via the Adams–Moulton method.[9] This finite difference method has been shown to converge to the exact solution as the net size is decreased to zero. Thus, we perform each computation (CV and SWV) over a range of net sizes and extrapolate the results to zero net size. We illustrate the accuracy achievable by this procedure by applying it to a particular SWV experiment that can be treated exactly.[10] This is the electrochemically reversible n-electron redox process

$$O + ne = R$$

The normalized peak current, $\Delta\psi_p$, for this redox process can be expressed as

$$\Delta\psi_p = (\Delta i_p/FAD_0^{1/2}C_0^b)(\pi t_p)^{1/2}$$

where $\Delta i_p/FAD_0^{1/2}C_0^b$ includes the diffusion coefficient and bulk concentration of the oxidized form and $(\pi t_p)^{1/2}$ includes the pulse width (t_p) of the square wave. Our simulation directly yields $\Delta i_p/FAD_0C_0^b$. Shown in Table II are our computed results for a one-electron process as a function of s (divisions per square-wave cycle) for a step height (ΔE_s) of 5 mV and a square-wave amplitude (E_{sw}) of 25 mV. The net size is inversely proportional to s as shown in Table II. When they are fit to a quadratic curve (i_{max} versus $1/s$), these data give a limiting value of 2.0161 at $1/s = 0$. The standard deviation is 2.2×10^{-5}. The value of $(\pi t_p)^{1/2}$ is 0.280 249, so that the value of $\Delta\psi_p$ is 0.5650. This is to be compared with the exact value of 0.5649. Table III summarizes the results for this and two other cases. As can be seen, the simulated results are in excellent agreement with the exact results. This extrapolation method is applied to all our CV and SWV computations.

Figure 1 shows the results of this method as applied to CV experiments (vide infra) where the complex (η-Cp)(CO)(PPh$_3$)FeMe (0.4 mM) is dissolved in methylene chloride (with 0.1 M TBAH at 0 °C) in the presence of 0.0308 M AN: i_1 and i_3 are the CV cathodic current peaks for the (η-Cp)(CO)(PPh$_3$)FeMe/(η-Cp)(CO)(PPh$_3$)FeMe$^+$ and the (η-Cp)(AN)(PPh$_3$)FeCOMe/(η-Cp)(AN)(PPh$_3$)FeCOMe$^+$ couples, respectively. The scan rate is 0.1 V s^{-1}; initial, vertex, and final potentials are −0.1, 0.5, and −0.5 V. For the simulations we use the following values: the heterogeneous rate constants $k_{h_1}D^{1/2}$ and $k_{h_3}D^{1/2}$ are 1.8 and 2.2 s$^{-1/2}$ cm^{-1}. The transfer coefficients α_1 and α_2 are each set at 0.5. Decomposition rate constants for (η-Cp)(CO)(PPh$_3$)FeMe$^+$ and (η-Cp)(AN)(PPh$_3$)FeCOMe$^+$ are 0.05 and 0 s^{-1}, respectively. Reduction potentials for the (η-Cp)(CO)(PPh$_3$)FeMe/(η-Cp)(CO)(PPh$_3$)FeMe$^+$ and (η-Cp)(AN)(PPh$_3$)FeCOMe/(η-Cp)(AN)(PPh$_3$)FeCOMe$^+$ couples are 0.265 and −0.355 V, respectively, versus a platinum pseudo reference electrode. Homogeneous rate constants k_2 and k_{-2} are 1.9×10^2 M^{-1} s^{-1} and 1.4 s^{-1}, respectively. The points for i_3/i_1 versus net size (inversely proportional to the number of divisions, n, of the total potential scan) were fit to a quadratic equation (standard deviation of the fit is 5×10^{-5}). The

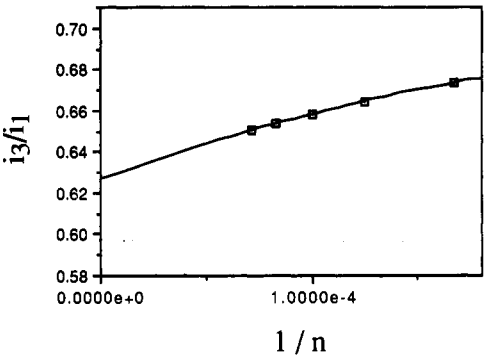

Figure 1. Plot of calculated i_3/i_1 versus net size ($1/n$). See text for details.

value of the intercept is what we seek: $i_3/i_1 = 0.626$. The same result is obtained by extrapolating i_3 and i_1 individually to zero net size and then taking the ratio.

Results

The electrochemistry of (η-Cp)(CO)(L)FeMe in acetonitrile differs from that in CH_2Cl_2.[1] In CH_2Cl_2, the CV's of (η-Cp)(CO)(L)FeMe show a normal set of anodic and cathodic waves for the (η-Cp)(CO)(L)FeMe/(η-Cp)(CO)(L)FeMe$^+$ couple. In contrast, in acetonitrile or solutions of acetonitrile in methylene chloride, the CV's (Figure 2) (scanning initially in the positive direction) of (η-Cp)(CO)(L)FeMe show an anodic wave for the (η-Cp)(CO)(L)FeMe/(η-Cp)(CO)(L)FeMe$^+$ couple. On the return scan, the cathodic wave for this couple might or might not be observed, depending on the nature of the ancillary ligands L, the scan rate of the experiments, and the concentration of acetonitrile. In addition, a second cathodic wave is observed about 0.6 V negative of the anodic wave for (η-Cp)(CO)(L)FeMe. Earlier,[11] in a study of the oxidation of (η-Cp)(CO)(PPh$_3$)FeMe in acetonitrile, we characterized the species responsible for the second oxidation wave as the acetonitrile complex (η-Cp)(AN)(PPh$_3$)FeCOMe$^+$. Since all the complexes in this study behave electrochemically in a manner similar to (η-Cp)(CO)(PPh$_3$)FeMe, we assume that they form complexes analogous to (η-Cp)(AN)(PPh$_3$)FeCOMe$^+$ on oxidation of (η-Cp)(CO)(L)FeMe in acetonitrile.

As further proof of the structure of (η-Cp)(AN)(L)FeCOMe$^+$, we checked the stoichiometry of the conversion of (η-Cp)(CO)(L)FeMe$^+$ to (η-Cp)(AN)(L)FeCOMe$^+$ for all complexes by measuring their relative concentrations as a function of [AN]. This was done by a series of electrochemical experiments which were performed in the following manner. The potential was stepped to a potential slightly positive of the anodic potential for (η-Cp)(CO)(L)FeMe and held there for 10 s. (Variation of the hold time over a range of 5–20 s made no significant change in the results of the experiments.) Holding for this period allows the complete oxidation of the material near the electrode surface. Immediately after the hold time, a linear sweep (scan rate 8.0 V s^{-1}) voltammogram was obtained by scanning from the hold potential in a negative direction to a final potential that was slightly negative of the reduction potential of (η-Cp)(AN)(L)FeCOMe$^+$. The relative currents of the cathodic waves (see Figure 3) for the re-

(9) Shampine, L. F.; Gordon, M. K. *Computer Solutions of Ordinary Differential Equations*; W. H. Freeman: San Francisco, CA, 1975.

(10) Osteryoung, J.; O'Dea, J. J. Square Wave Voltammetry. In *Electroanalytical Chemistry*; Bard, A. J., Ed., Marcel Dekker: New York, 1986; Vol. 14.

(11) Magnuson, R. H.; Meirowitz, R. E.; Zulu, S. J.; Giering, W. P. *J. Am. Chem. Soc.* **1982**, *104*, 5790.

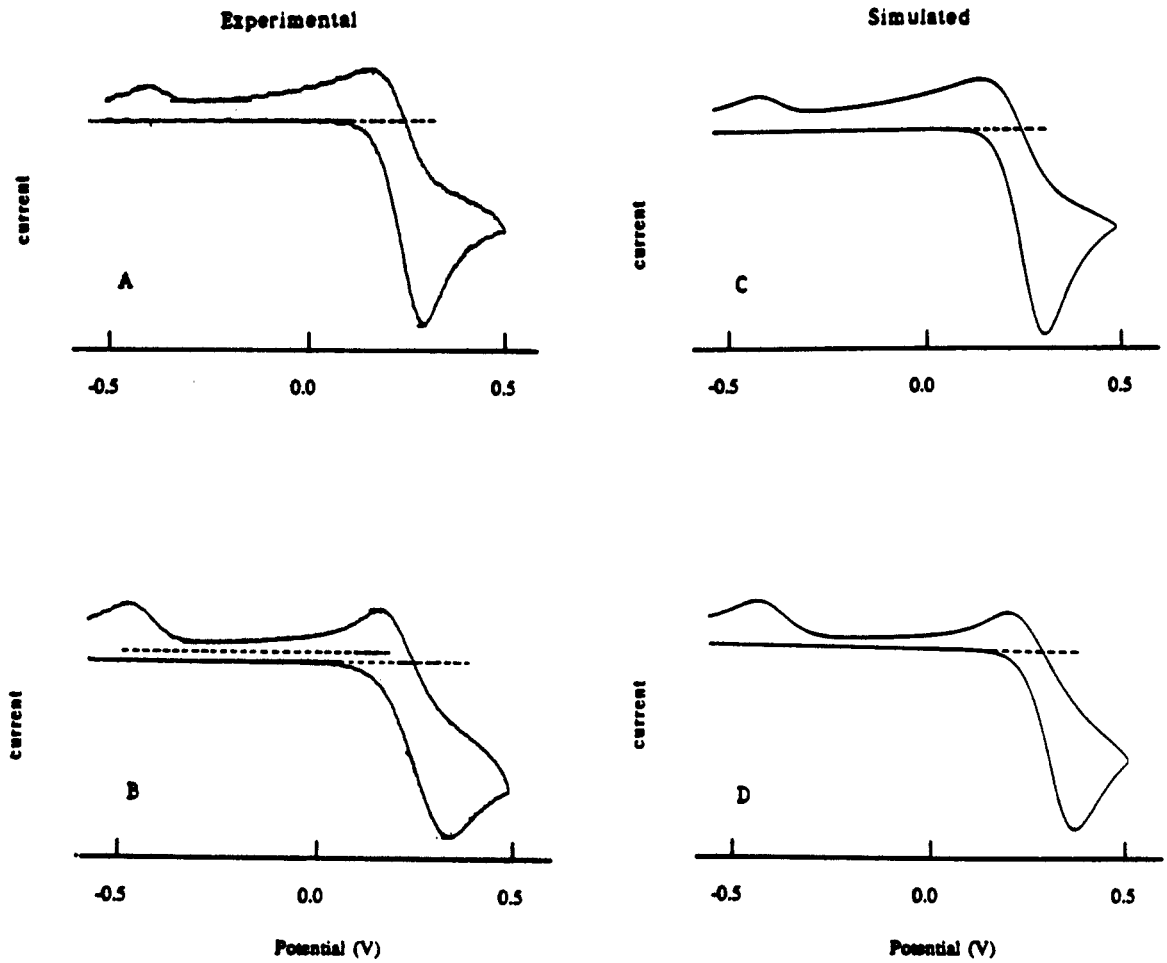

Figure 2. Simulated and experimental CV's for (η-Cp)(CO)(PPh_3)FeMe as measured in CH_2Cl_2 containing 0.1 M TBAH and 0.0308 mM AN at 0 °C. Curves a and c correspond to a scan rate of 0.1 V s^{-1}; curves b and d correspond to a scan rate of 1.6 V s^{-1}.

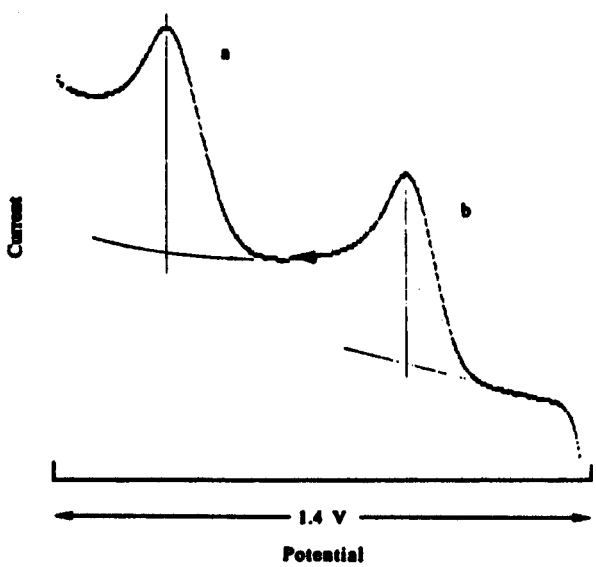

Figure 3. Linear sweep voltammograms of (η-Cp)(CO)(PEt_3)FeMe in CH_2Cl_2 containing 0.231 mM AN. The experiment was performed by holding the electrode potential to the positive side of $E^{\circ\prime}$ for the oxidation of (η-Cp)(CO)(PEt_3)FeMe for 10 s and then sweeping in the negative direction at 8 V s^{-1}. Peaks a and b result from the reduction of (η-Cp)(AN)(PEt_3)$FeCOMe^+$ and (η-Cp)(CO)(PEt_3)$FeMe^+$, respectively. The auxiliary base line drawn under peak a follows that of peak b in the absence of acetonitrile. See text for details.

duction of residual (η-Cp)(CO)(L)$FeMe^+$ and (η-Cp)(AN)(L)$FeCOMe^+$ were readily measured and found to be invariant at scan rates above 4.0 V s^{-1}. Plots (Figure 4)

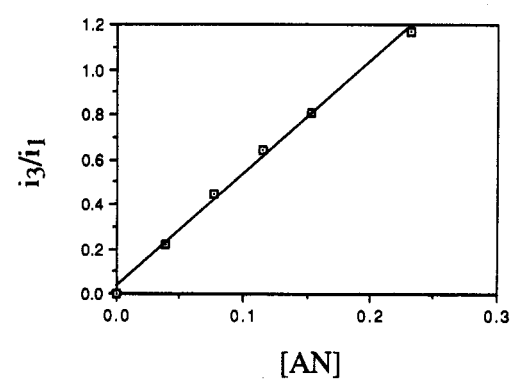

Figure 4. Plot of the CV current ratios for the reduction of (η-Cp)(AN)(PEt_3)$FeCOMe^+$ (i_3) and (η-Cp)(CO)(PEt_3)$FeMe^+$ (i_1) versus [AN]. Details of the experiment are given in the Results section. $i_3/i_1 = 5.04[AN] + 0.031$; $r^2 = 0.996$.

of the ratios of the currents for the cathodic waves ((η-Cp)(AN)(L)$FeCOMe^+$ and (η-Cp)(CO)(L)$FeMe^+$) versus [AN] were linear. This linearity indicates a 1:1 stoichiometry between (η-Cp)(CO)(L)$FeMe^+$ and AN. All the complexes used in this study behave in this manner. The slope of these graphs afforded estimated equilibrium constants (Table I) that are close to those obtained by the simulation methods (vide infra). (The rate constants derived via simulation were used in the simulations of other electrochemical experiments from which kinetic data were determined; vide infra.)

As mentioned above, the CV's of (η-Cp)(CO)(L)FeMe in acetonitrile or mixtures of acetonitrile in methylene chloride were dependent on the nature of L, the scan rate,

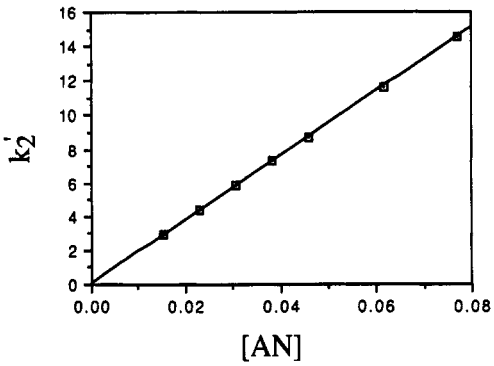

Figure 5. Plot of the pseudo-first-order rate constant k_2' versus [AN] for (η-Cp)(CO)(PPh_3)FeMe. $k_2' = 189[AN] + 0.003$; $r^2 = 1.00$.

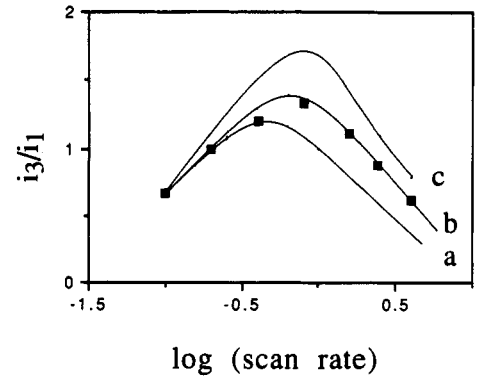

Figure 6. Plot of i_3/i_1 as a function of log (scan rate) for (η-Cp)(CO)(PPh_3)FeMe. Calculated ratios are shown as curves, whereas experimental data are shown as filled squares. i_3 and i_1 correspond to the reduction of (η-Cp)(AN)(PPh_3)$FeCOMe^+$ and (η-Cp)(CO)(PPh_3)$FeMe^+$, respectively. Curves a–c are calculated ratios for k_2/k_{-2} ratios of 1.1×10^2, 1.4×10^2, and 1.6×10^2, respectively.

and [AN] (Figure 2). CV experiments, as described below for (η-Cp)(CO)(PPh_3)FeMe, allow us to determine the rate constants k_2 and k_{-2} for the interconversion of (η-Cp)(CO)(L)$FeMe^+$ and (η-Cp)(AN)(L)$FeCOMe^+$ (Scheme I) by computer simulation. In undiluted acetonitrile, the anodic wave for (η-Cp)(CO)(PPh_3)FeMe is observed; however, a corresponding cathodic wave is not observed since (η-Cp)(CO)(PPh_3)$FeMe^+$ is quantitatively and rapidly converted to (η-Cp)(AN)(PPh_3)$FeCOMe^+$. A reduction wave for (η-Cp)(AN)(PPh_3)$FeCOMe^+$ is observed about 0.6 V negative of the anodic wave for (η-Cp)(CO)(PPh_3)FeMe. At much lower concentrations of AN (0.03 M) in CH_2Cl_2, the CV's are very scan rate dependent. Thus, at low scan rates (50 mV s^{-1}) the cathodic wave for the reduction of (η-Cp)(CO)(PPh_3)$FeMe^+$ is large, whereas the cathodic wave for the reduction of (η-Cp)(AN)(PPh_3)$FeCOMe^+$ is small. At intermediate scan rates (1.0 V s^{-1}), the cathodic wave for the reduction of (η-Cp)(CO)(PPh_3)$FeMe^+$ and (η-Cp)(AN)(PPh_3)$FeCOMe^+$ are of comparable current. Finally, at high scan rates (8.0 V s^{-1}), the cathodic wave for (η-Cp)(CO)(PPh_3)$FeMe^+$ is much larger than the wave for (η-Cp)(AN)(PPh_3)$FeCOMe^+$. This is the behavior expected when the scan rate of the CV experiment is competitive with the rates of interconversion of (η-Cp)(CO)(PPh_3)$FeMe^+$ and (η-Cp)(AN)(PPh_3)$FeCOMe^+$. This behavior is observed at low concentrations of acetonitrile when L is a small and poor electron donor ligand and at high concentrations of AN when L is a large and basic ligand. (In fact, for (η-Cp)(CO)(PCy_3)FeMe it is necessary to perform the CV experiment in undiluted acetonitrile in order to observe the aforementioned phenomenon.)

Measurement of k_2 and k_{-2}. We used cyclic voltammetry to measure the forward and backward rate constants (and their ratio, K_{eq}) between (η-Cp)(CO)(L)$FeMe^+$ and (η-Cp)(AN)(L)$FeCOMe^+$. Solutions consist of known amounts of (η-Cp)(CO)(L)FeMe and acetonitrile in methylene chloride containing 0.1 M TBAH at 0 °C. CV's were taken over a potential range encompassing the oxidation of the starting material and its reduction along with the reduction of (η-Cp)(AN)(L)$FeCOMe^+$ formed in the process. For (η-Cp)(CO)(PPh_3)FeMe, pseudo-first-order rate constants, k_2' and k_{-2}' were determined by computer simulation as a function of acetonitrile concentration, which was varied over a 5-fold range. A plot (Figure 5) of k_2' versus [AN] is linear, indicating that the reaction is second order. k_{-2}' is independent of [AN]. For the remainder of the complexes, we found it useful to select a single acetonitrile concentration which produced nearly equal peak cathodic currents for (η-Cp)(CO)(L)$FeMe^+$ and (η-Cp)(AN)(L)$FeCOMe^+$ at a sweep rate of 1.0 V s^{-1}. Figure 2 shows a comparison between experimental and simulated results for the complex (η-Cp)(CO)(PPh_3)FeMe at two scan rates. Curves A and C correspond to a sweep rate of 0.1 V s^{-1}, and B and D correspond to a sweep rate of 1.6 V s^{-1}. We corrected the return wave of each experimental CV for capacitive current by redrawing the base line at a level consistent with the height of the minimum above the base line in the simulated curves. We point out that this method is effective because the height of the computed minimum is quite insensitive to the value selected for k_2 and k_{-2} over a wide range around the final values of k_2 and k_{-2}. For the slower sweep rate this auxiliary line is indistinguishable from the base line. The currents i_1 (reduction of (η-Cp)(CO)(L)$FeMe^+$) and i_3 (reduction of (η-Cp)(AN)(L)$FeCOMe^+$) are measured from this base line.

Figure 6 shows the result of our fit to the data of i_3/i_1 for three nearby ratios of k_2/k_{-2}. For a given value of k_2/k_{-2} a value of k_{-2} is found which reproduces the experimental i_3/i_1 at the slowest scan rate (here, 0.1 V s^{-1}). The rest of the curve is generated using these values of k_2 and k_{-2}. Scan rates range over a factor of 40, and this is large enough for us to discriminate between the quality of fits.

Experiments with (η-Cp)(CO)(P(*i*-Pr)$_3$)FeMe showed that the calculated rate constants (k_2 and k_{-2}) for the interconversion of (η-Cp)(CO)(P(*i*-Pr)$_3$)$FeMe^+$ and (η-Cp)(AN)(P(*i*-Pr)$_3$)$FeCOMe^+$ changed insignificantly (around 10%) when measured in 40% (by volume) AN in CH_2Cl_2 and 100% AN, respectively. Thus, we believe the rate constants measured in different solvent mixtures can be compared. The rate constants k_2 and k_{-2} along with K_{eq} are shown in Table I.

Determination of k_5. The CV's of (η-Cp)(CO)(L)FeMe, when measured in acetonitrile saturated with CO, show waves for the oxidation of (η-Cp)(CO)(L)FeMe and (η-Cp)(CO)(L)FeCOMe. (η-Cp)(CO)(L)FeCOMe is formed by the electrochemically initiated, redox-catalyzed carbonylation of (η-Cp)(CO)(L)FeMe is shown in Scheme I.

The rate constants for the reactions between (η-Cp)(AN)(L)$FeCOMe^+$ and CO were determined by computer simulation of square-wave voltammetry experiments (Figure 7). The experiments were performed on acetonitrile solutions containing 0.1 M TBAH and about 0.2–0.7 mM (η-Cp)(CO)(L)FeMe. The concentration of CO was always at least 8 times greater than the concentration of complex. The SWV anodic current ratios for the oxidation of (η-Cp)(CO)(L)FeMe and (η-Cp)(CO)(L)FeCOMe were routinely measured as a function of the concentration of CO (50%, 75%, and 100%) in argon. Plots of percent CO

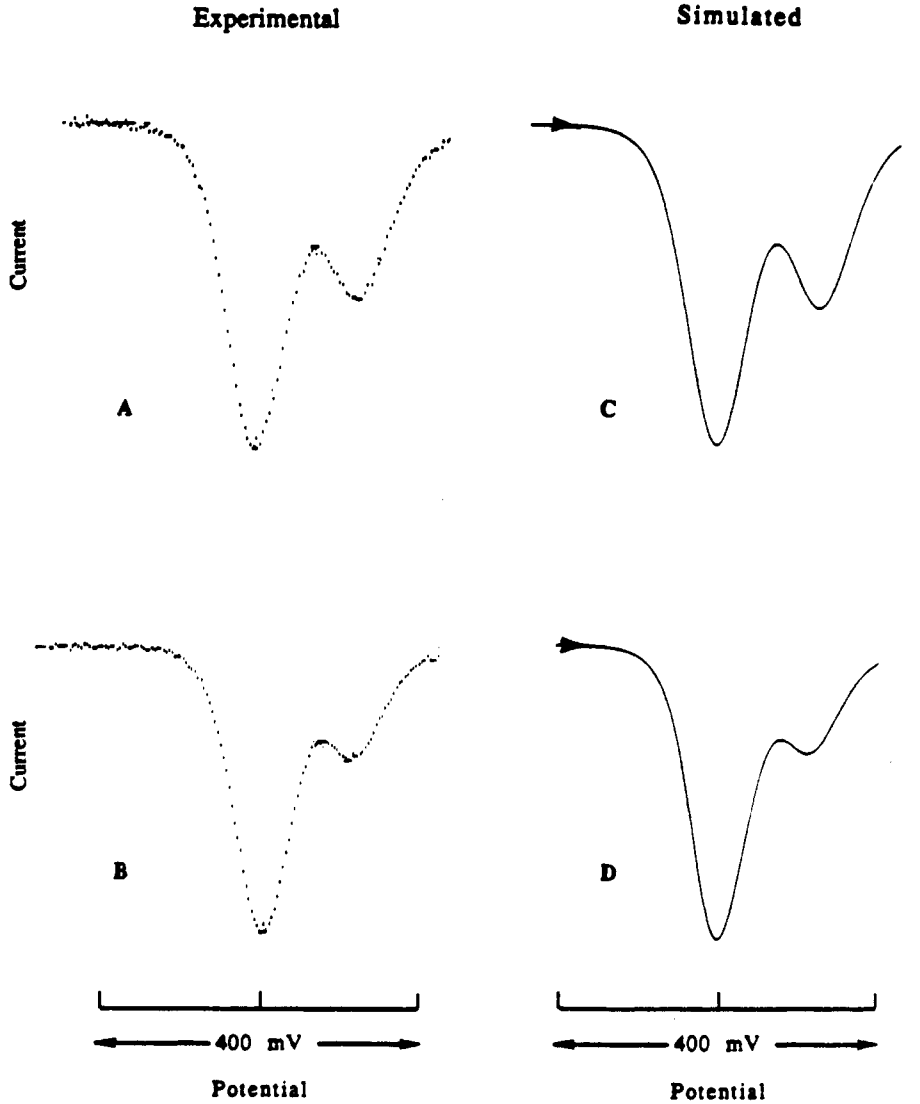

Figure 7. Simulated and experimental square-wave voltammograms for (η-Cp)(CO)(P(i-Pr)$_3$)FeMe in acetonitrile saturated with CO at 1 atm and 0 °C. The scan rate was 4 mV s^{-1} in parts a and c and 8 mV s^{-1} in parts b and d. The first peak corresponds to the oxidation of (η-Cp)(CO)(P(i-Pr)$_3$)FeMe, and the more positive peak corresponds to the oxidation of (η-Cp)(CO)(P(i-Pr)$_3$)FeCOMe formed during the experiment by the electrochemically promoted carbonylation of (η-Cp)(CO)(P(i-Pr)$_3$)FeMe.

versus current ratio (i_2/i_1) were linear and passed through the origin, thereby indicating that the reactions were first order in CO. In simulating the carbonylation experiments, we used the values for k_2 and k_{-2} obtained from CV experiments and then varied the values of k_5 until a satisfactory simulation was achieved. A particular case is discussed next.

Our analysis for the rate of reaction of (η-Cp)(AN)(L)FeCOMe$^+$ with CO takes into account the kinetics of formation of (η-Cp)(AN)(L)FeCOMe$^+$ as shown in Scheme I. It turns out that only for (η-Cp)(AN)(L)FeCOMe$^+$ with the slowest rates of formation is this necessary. Such a complex is (η-Cp)(CO)(P(i-Pr$_3$))FeMe. Figure 7 shows experimental and simulated SWV data for carbonylation of a 0.5 mM solution of the complex (η-Cp)(CO)(P(i-Pr$_3$))FeMe in acetonitrile at 0 °C: k_2 and k_{-2} are 0.9 M^{-1} s^{-1} and 6.5 s^{-1}, respectively, as obtained from the CV analysis described above. The best fit was obtained when we used the following values: heterogeneous rate constants of $k_{h_1}D^{1/2}$ and $k_{h_2}D^{1/2}$ are 2.0 and 2.4 s$^{-1/2}$ cm^{-1}, respectively, and both α values are 0.5. The $E^{\circ\prime}$ values for the (η-Cp)(CO)(P(i-Pr)$_3$)FeMe/(η-Cp)(CO)(P(i-Pr)$_3$)FeMe$^+$ and (η-Cp)(CO)P(i-Pr)$_3$)FeCOMe/(η-Cp)(CO)(P(i-Pr)$_3$)FeCOMe$^+$ couples are 0.160 and 0.270 relative to a platinum pseudo reference electrode. k_{et} is taken to be greater than 10^4 M^{-1} s^{-1}. This is consistent with the magnitude of electron-transfer rates found for these complexes in methylene chloride.[1] Values larger than this give essentially the same results for these scan rates (vide infra). k_5 turns out to be 8.2 M^{-1} s^{-1} (±10%).

The value derived for k_5 is quite insensitive to variations (by the same factor) in $k_{h_1}D^{1/2}$ and $k_{h_2}D^{1/2}$ within wide ranges. For example, for a 5-fold change in $k_{h_1}D^{1/2}$ and $k_{h_2}D^{1/2}$ (from 2.0 and 2.4 to 10 and 12 s$^{-1/2}$ cm^{-1}, respectively) and an independent 20-fold change in k_{et} (5×10^3–1×10^5 M^{-1} s^{-1}) the best values of k_5 based on peak current ratios vary only from 8.2 to 9.0 M^{-1} s^{-1}. (For the SWV experiments we regard currents below the base line as positive. Then we can describe our results in terms of two peak currents with a valley between them.) Furthermore, we find that these variations of $k_{h_1}D^{1/2}$ and $k_{h_2}D^{1/2}$ or of k_{et} have a considerably larger effect on the relative depth of the valley between the peaks than they do on the ratio of peak heights. This is fortunate because variation of k_5 has the opposite effect: it affects the ratio of peak heights more than it affects the depth of the valley. For example, using the extreme values of 10 and 12 for $k_{h_1}D^{1/2}$ and $k_{h_2}D^{1/2}$, and with k_{et} being either 5×10^3 or 1×10^5 M^{-1} s^{-1}, we find that the depths of the minima between current peaks for both scan rates are 25% too small, a detectably

poorer fit. In this manner, we are able to reject values for k_5 of 8.5 M^{-1} s^{-1} and larger. A pertinent discussion of error introduced by uncertainties in $k_{b_1}D^{1/2}$ and $k_{b_2}D^{1/2}$, as well as transfer coefficients α is also found in ref 1.

If we assume for this system that formation of (η-Cp)(AN)(L)FeCOMe$^+$ (Scheme I) is very fast, essentially regarding k_5 as rate determining, then we still get nearly the same quality of fit but a lower value of k_5. Instead of 8.2 we get 6.0 M^{-1} s^{-1}, a value around 30% lower. This difference is significant but small enough so that we can assert that the derived k_5 value is not very sensitive to error in the rate constants for formation of (η-Cp)(AN)(L)FeCOMe$^+$ from (η-Cp)(CO)(L)FeMe$^+$.

We quantitatively analyzed the equilibrium and kinetic data obtained from the aforementioned experiments in terms of the stereoelectronic properties of the phosphorus(III) ligands as previously described.[12] The data for two complexes did not always correlate with the remainder. Both (η-Cp)(CO)(PEt_3)FeMe$^+$ and (η-Cp)(CO)(P(*i*-Bu)$_3$)FeMe$^+$ were unusually unreactive toward carbonylation in CH_2Cl_2 (k_1). (η-Cp)(CO)(P(*i*-Bu)$_3$)FeMe$^+$ was also unusually unreactive toward carbonylation in AN (k_5), where it should have been one of the most reactive complexes. In the k_2 and k_{-2} steps, the two complexes behaved normally.

Discussion

AN-Assisted Alkyl to Acyl Rearrangement: k_2 and k_{-2} Steps. The kinetic data are consonant with the alkyl to acyl rearrangement of (η-Cp)(CO)(L)FeMe$^+$ in acetonitrile (k_2 step) being nucleophilically assisted by an entering molecule of solvent, whereas the reverse reaction, the k_{-2} step, is independent of [AN]. The K_{eq} values for (η-Cp)(CO)(L)FeMe$^+$/(η-Cp)(AN)(L)FeCOMe$^+$ equilibria are very dependent on the nature of L and vary by a factor of 40000, from 0.071 to 3×10^3 M^{-1} for L = PCy_3 and P(*p*-$CF_3Ph)_3$, respectively. The electronic profile[12] of K_{eq} (Figure 8, plot of log K_{eq} versus the electronic parameter, χ) exhibits a very strong dependence on the electron-donor capacity of L, with poorer electron donor ligands associated with a larger K_{eq}. The line in Figure 8a is drawn through the data for the complexes containing the isosteric ligands P(*p*-$XC_6H_4)_3$. A steric profile (Figure 8b) is constructed[12] by plotting, versus θ, the deviations from this line of the data for the other complexes. Steric profiles display the manner in which thermodynamic (or kinetic) properties of a reaction respond to changes in the size of L. The steric profile of log K_{eq} shows that log K_{eq} becomes smaller as the size of L increases—(η-Cp)(AN)(L)FeCOMe$^+$ is more congested than (η-Cp)(CO)(L)FeMe$^+$. The steric effect is small compared to the electronic effect and varies by a factor of 30 on going from the complex containing the smallest (L = PMe_3) ligand to the complex containing the largest (L = PCy_3) ligand.

Examination of the electronic and steric profiles of the second-order forward (k_2) and first-order reverse (k_{-2}) rate

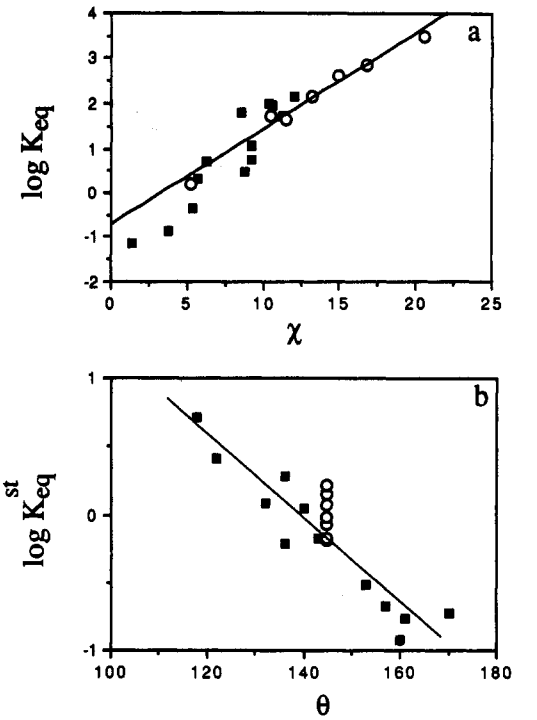

Figure 8. (a) Plot of log K_{eq} for the interconversion of (η-Cp)(CO)(L)FeMe$^+$ and (η-Cp)(AN)(L)Fe(CO)Me$^+$ versus the electronic parameter χ (electronic profile). The best-fit line is drawn through the points (open circles) for the complexes containing the isosteric ligands P(*p*-$XC_6H_4)_3$ (log K_{eq} = 0.214χ − 0.731, r^2 = 0.978). (b) Plot of the deviations (log K_{eq}^{st}) of the data in Figure 8a from the best-fit line for the data for the complexes containing P(*p*-$XC_6H_4)_3$ versus cone angle θ (steric profile). The best-fit line for *all* log K_{eq}^{st} values is shown (log K_{eq}^{st} = −0.030θ + 4.22, r^2 = 0.793). The data for P(*p*-$XC_6H_4)_3$ are shown as open circles.

constants for the equilibrium between (η-Cp)(CO)(L)FeMe$^+$ and (η-Cp)(AN)(L)FeCOMe$^+$ (Figure 9) shows us that k_{-2} varies over a much smaller range than k_2 so that variations in K_{eq} almost parallel k_2. A plot of log k_2 versus log K_{eq} for the data for the isosteric triaryl complexes (line in Figure 10a) allows a direct comparison between log k_2 and log K_{eq} without complicating steric factors. The slope of the line is 0.73, which indicates that the transition state is more like the product that the reactant. A plot (Figure 10b) of the steric component of log k_2 versus the steric component of log K_{eq} gives a linear plot with a slope of 0.78, which suggests that the steric factors are similar but somewhat less severe in the transition state than in (η-Cp)(AN)(L)FeCOMe$^+$. In comparison, the slope of the linear plot of log k_{-2} versus log K_{eq} is rather shallow and negative, consonant with a transition state that is slightly less electron rich than (η-Cp)(AN)(L)FeCOMe$^+$. A similar plot of the steric component of log k_{-2} (log k_{-2}^{st}) versus the steric component of log K_{eq} (log K_{eq}^{st}) exhibits a small negative slope, indicating that the transition state is only slightly less congested than (η-Cp)(AN)(L)FeCOMe$^+$. From these observations we envision a transition state that contains an extensively formed acetyl ligand with an entering AN ligand. This transition state is similar to the one we proposed for the CH_2Cl_2-induced alkyl to acyl rearrangement, except the AN ligand is more strongly bonded.

It is insightful at this juncture to compare the kinetics of the CH_2Cl_2- (k_1) and AN-induced (k_2) rearrangements of (η-Cp)(CO)(L)FeMe$^+$. The steric and electronic profiles (parts a and b of Figure 11) for the k_1 step were constructed from the data in Table I. The data for the com-

(12) (a) Liu, H.-Y.; Eriks, E.; Prock, A.; Giering, W. P. *Acta Crystallogr.* **1990**, *C46*, 51–54. (b) Panek, J.; Prock, A.; Eriks, K.; Giering, W. P. *Organometallics* **1990**, *9*, 2175. (c) Liu, H.-Y.; Eriks, E.; Prock, A.; Giering, W. P. *Organometallics* **1990**, *9*, 1758. (d) Eriks, K.; Liu, H.-Y.; Koh, L.; Prock, A.; Giering, W. P. *Acta Crystallogr.* **1989**, *C45*, 1683–1686. (e) Rahman, M. M.; Liu, H.-Y.; Eriks, K.; Prock, A.; Giering, W. P. *Organometallics* **1989**, *8*, 1–7. (f) Rahman, M. M.; Liu, H.-Y.; Prock, A.; Giering, W. P. *Organometallics* **1987**, *6*, 650–658. (g) Golovin, M. N.; Rahman, M. M.; Belmonte, J. E.; Giering, W. P. *Organometallics* **1985**, *4*, 1981–1991. (h) Lezhan, C.; Poe, A. J. *Inorg. Chem.* **1989**, *28*, 3641. (i) Brodie, N. M.; Chen, L.; Poe, A. J. *Int. J. Kinet.* **1988**, *27*, 188. (j) Poe, A. J. *Pure Appl. chem.* **1988**, *60*, 1209. (k) Dahlinger, K.; Falcone, F.; Poe, A. J. *Inorg. Chem.* **1986**, *25*, 2654. (l) Eriks, E.; Liu, H.-Y.; Prock, A.; Giering, W. P. *Inorg. Chem.* **1989**, *28*, 1759–1763.

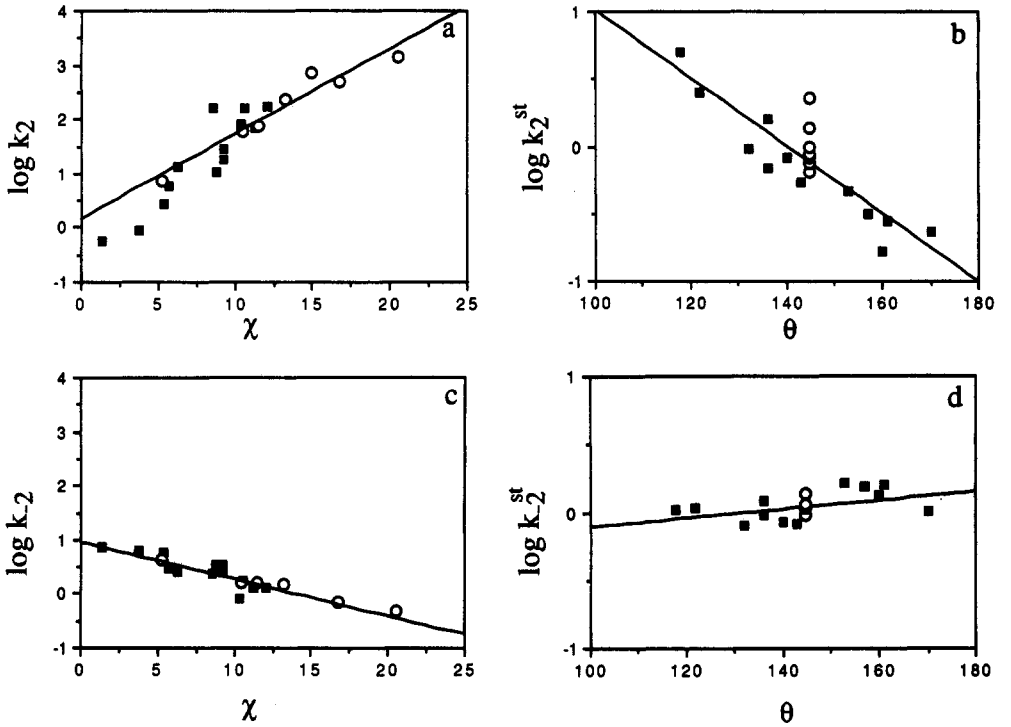

Figure 9. (a, c) Electronic profiles of k_2 and k_{-2}, respectively. The best-fit lines are drawn through the data for the complexes containing the P(*p*-$XC_6H_4)_3$ ligands (open circles): $\log k_2 = 0.16\chi + 0.15$, $r^2 = 0.944$; $\log k_{-2} = -0.068\chi + 0.94$, $r^2 = 0.78$. (b, d) Steric profiles of k_2 and k_{-2}, respectively. The best-fit lines are drawn through the data for all the complexes: $\log k_2^{st} = -0.025\theta + 3.54$, $r^2 = 0.75$; $\log k_{-2}^{st} = 0.003\theta = 0.043$, $r^2 = 0.091$. (The small value of r^2 reflects the small gradient of the plot.)

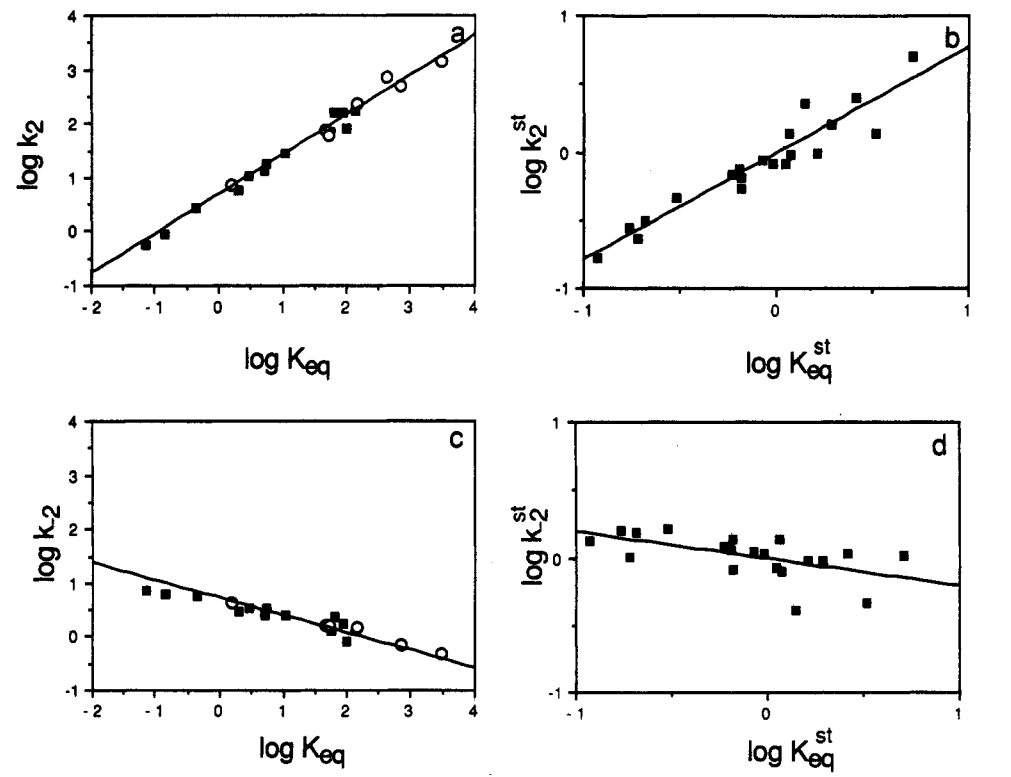

Figure 10. Plots of log k_2 (a) and log k_{-2} (c) versus log K_{eq} plots of the steric components log k_2^{st} (b) and k_{-2}^{st} (d) versus log K_{eq}^{st}. The best-fit lines in (a) and (c) are drawn through the data (open circles) for the complexes containing the isosteric ligands, P(*p*-$XC_6H_4)_3$: $\log k_2 = 0.73(\log K_{eq}) + 0.68$, $r^2 = 0.972$; $\log k_{-2} = -0.32(\log K_{eq}) + 0.72$, $r^2 = 0.83$). The best-fit lines in (b) and (d) are drawn through all the data: $\log k_2^{st} = 0.78(\log K_{eq}^{st}) - 0.016$, $r^2 = 0.90$; $\log k_{-2}^{st} = -0.20(\log K_{eq}^{st}) - 0.01$, $r^2 = 0.31$.

plexes containing the PPh_2Et, P(*i*-Bu)$_3$, PPh_2-*t*-Bu, and P(*i*-Pr)$_3$ ligands are reported for the first time in this paper. Electronically, the two reactions (k_1 and k_2 steps) behave in a similar manner, in that both exhibit a rate enhancement as the electron-donor capacity of L decreases, thereby indicating a transition state that is more electron rich than (η-Cp)(CO)(L)$FeMe^+$. This is not surprising, since in both transition states the strong π-acid ligand CO is being replaced by an electron-donor ligand, either AN or CH_2Cl_2. In addition, the methyl ligand is being replaced by an acetyl ligand, which exhibits about the same electron-donor capacity, as shown by the similarities of the terminal

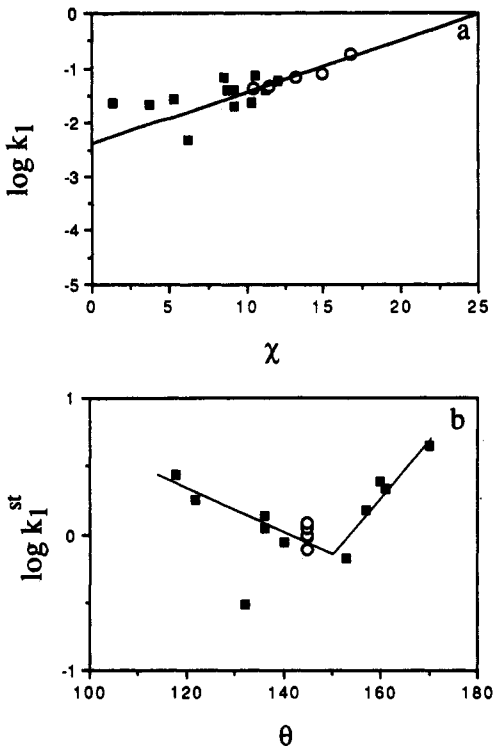

Figure 11. (a) Electronic (a) and steric profiles (b) of k_1 for the reaction between CH_2Cl_2 and (η-Cp)(CO)(L)FeMe$^+$. The best-fit line in the electronic profile is drawn through the points for the complexes containing the isosteric ligands P(*p*-$XC_6H_4)_3$ (open circles): $\log k_1 = 0.094\chi - 2.41$, $r^2 = 0.92$. The point far off the steric profile corresponds to the data point for the PEt_3 complex.

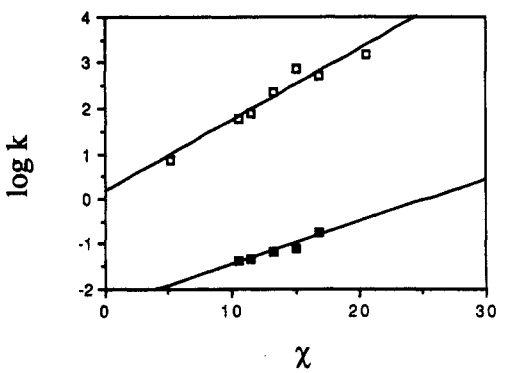

Figure 12. Plots of log k_1 (filled squares) and log k_2 (open squares) versus the electronic parameter χ. Only the data for the complexes containing the P(*p*-$XC_6H_4)_3$ ligands are displayed.

carbonyl stretching frequencies of complexes such as (η-Cp)(CO)(L′)FeMe and (η-Cp)(CO)(L′)FeCOMe (L′ = PPh_3, CO).[12e,g] Plots of log k_2 and log k_1 for the triaryl ligands (Figure 12) versus χ reveal that the acetonitrile reactions are a few orders of magnitude faster than the analogous CH_2Cl_2 reactions. In addition, the slope of the acetonitrile plot is steeper than that of the CH_2Cl_2 plot, indicating that acetonitrile is probably more strongly bonded than the less nucleophilic CH_2Cl_2 (or PF_6^-) in the transition state.

The steric profiles of the k_1 and k_2 steps (Figures 11b and 9b, respectively) appear to be different, and this presents a problem. The steric profile of the k_1 step shows a region at small θ where there is steric inhibition of the reaction, which must be associated with congestion in the transition state. At about 150° there is a steric threshold and the reaction becomes sterically accelerated for ligands with $\theta > 150°$. We suggested that this steric threshold corresponds to the onset of steric effects in (η-Cp)(CO)(L)FeMe$^+$. In principle, this steric threshold should be manifest in any process (i.e. log K_{eq} and log k_2) that involves (η-Cp)(CO)(L)FeMe$^+$. The steric profile of the k_2 (and of the K_{eq}) step should show a threshold near 150°; if it is there, it is not obvious. This could happen because the steric components of K_{eq} and k_2 are overwhelmed by the electronic contributions (see Figures 8 and 9). Hence, the errors in the evaluation of the electronic contribution are probably large compared to the small steric contribution. Thus, the steric profiles, which include all the errors in the analysis, show considerable scatter. There appears, however, to be fine structure hidden in the steric profiles (Figures 8b and 9b). First, inspection of the profiles suggests that there is curvature to the plots, with the gradient becoming less steep at larger θ. Second, linear regression analysis seems to confirm this observation, since a only a poor fit ($r^2 = 0.79$) of a line to the data is obtained. Third, all the data for the complexes containing the triaryl ligands lie above the best-fit line in steric profiles of both K_{eq} and k_2. At present, the best we can say about the steric profiles of K_{eq} and k_2 is that they show steric inhibition.

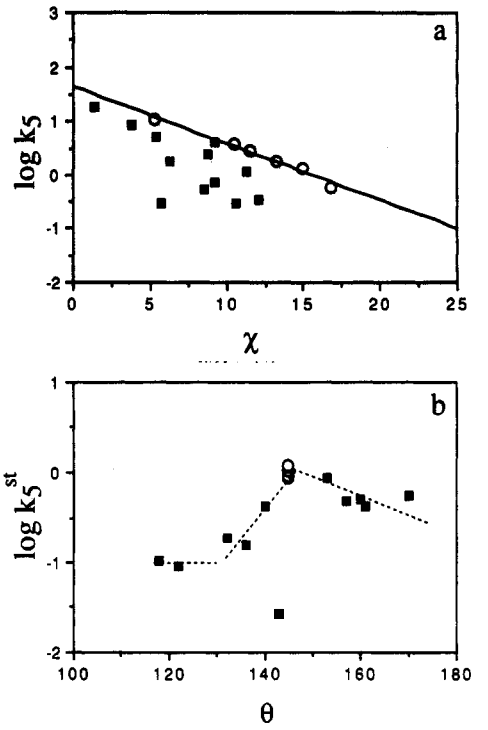

Figure 13. Electronic (a) and steric profiles (b) for the k_5 step in Scheme I. The best-fit line in (a) is drawn through the data for the complexes containing the isosteric P(*p*-$XC_6H_4)_3$ ligands, which are shown as open circles. $\log k_5 = -0.106\chi + 1.64$, $r^2 = 0.984$.

Several years ago Trogler[6] presented convincing evidence for the rapid formation of the transient, formally heptacoordinate methyl complex (η-Cp)(CO)(py)(L)FeMe$^+$ during the pyridine-promoted alkyl to acyl rearrangement of (η-Cp)(CO)(PPh_3)FeMe$^+$:

(η-Cp)(CO)(PPh_3)FeMe$^+$ + py → (η-Cp)(CO)(py)(PPh_3)FeMe$^+$ → (η-Cp)(py)(PPh_3)FeCOMe$^+$

Although we have found no evidence for an analogous hepatacoordinate intermediate during the carbonylation of (η-Cp)(CO)(L)FeMe$^+$ in either CH_2Cl_2 or AN, we do not believe that our observations are inconsistent with Trogler's. We have observed that both k_1 and k_2 are diminished as the electron-donor capacity of the phosphine ligands increases. In part, this is attributable to the formation of a transition state that is more electron rich than

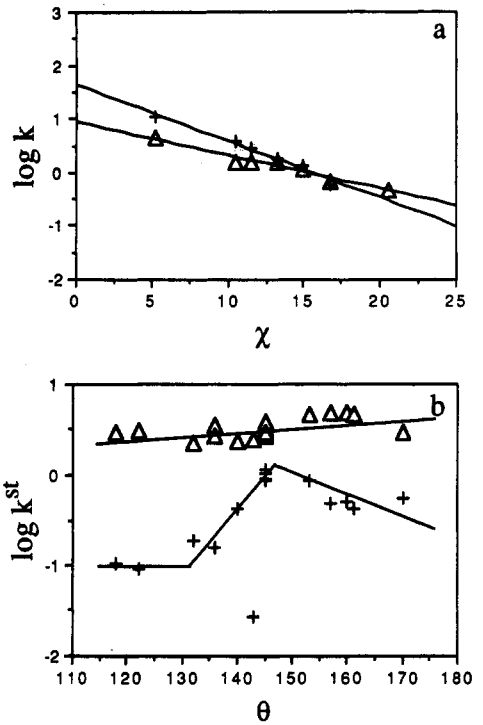

Figure 14. Comparison of the electronic profiles (for complexes containing the isosteric $P(p\text{-}XC_6H_4)_3$ ligands only) (a) and the steric profiles (b) for the k_{-2} and k_5 steps of Scheme I. Data for the k_5 step are shown as crosses, and data for the k_{-2} step are shown as open triangles. For clarity, a constant of 0.5 was added to log k_{-2}^{st}.

the ground state (vide supra). In addition, the better electron donor ligands probably stabilize the ground state by enhancing Fe–CO back-bonding. The entering ligand (CH_2Cl_2, AN, or py) can also modify the electron density on the iron and thereby effect the Fe–CO bond. The best electron donor entering ligand (py) could enhance Fe–CO back-bonding to the extent that the alkyl to acyl rearrangement is stopped during the addition of the nucleophile. Since both CH_2Cl_2 and AN are poorer electron donors, the addition of the entering ligand and the rearrangement might occur in a concerted manner.

Carbonylation of (η-Cp)(AN)(L)FeCOMe$^+$: k_5 Step. Several modes of carbonylation of (η-Cp)(AN)(L)FeCOMe$^+$ can be envisioned. The involvement of (η-Cp)(CO)(L)FeMe$^+$ in the carbonylation can be discounted, since this complex, which is the dominant iron(III) reactant[1] in CH_2Cl_2, where it shows no appreciable reactivity toward CO, is present in very low concentrations for most of the complexes in undiluted acetonitrile. The conversion of (η-Cp)(AN)(L)FeCOMe$^+$ to (η-Cp)(CO)(L)FeCOMe$^+$ might involve a direct displacement of AN by CO from (η-Cp)(AN)(L)FeCOMe$^+$ or a rapid preequilibrium between (η-Cp)(AN)(L)FeCOMe$^+$ and a transient complex such as the η^2-acyl complex (η-Cp)(L)Fe(η^2-COMe)$^+$, (η-Cp)(CH_2Cl_2)(L)FeCOMe$^+$, or (η-Cp)(PF_6)(L)FeCOMe followed by incorporation of CO. We have recently completed studies on the carbonylation of (η-Cp)(AN)(L)FeCOMe$^+$ in CH_2Cl_2 as a function of [AN]. The results of these experiments, which have been submitted for publication, suggest that indeed a preequilibrium is involved, although the nature of the intermediate is problematic.

Even though the k_5 step appears to be a multistep process, analysis of its electronic and steric profiles is insightful. The electronic profile (Figure 13a) shows that the reaction is accelerated by the better electron donor ligands. The steric profile (Figure 13b) is complex and shows at least one steric threshold at 146° and possibly another around 133°. Thus, between 118 and 133° there appears to be a region of no steric effects. From 135 to 146° there is steric acceleration. At still larger L, there is a small steric inhibition of the reaction.

Although both the k_5 and k_{-2} steps involve the dissociation of AN, comparison of their respective electronic and steric profiles reveals that they are very different processes. Plots of log k_{-2} and log k_5 versus χ for the complexes containing the isosteric triaryl ligands (Figure 14) reveals that each step involves a transition state which is electron-deficient in comparison to (η-Cp)(AN)(L)FeCOMe$^+$; however, the k_5 step is more sensitive to variations in the electron-donor capacity of L. The steric profiles show that little of the steric effect in (η-Cp)(AN)(L)FeCOMe$^+$ is relieved in the k_{-2} step as compared to the k_5 step, which shows a rather dramatic steric acceleration, especially between 133 and 146°. Thus, it appears that the k_{-2} and k_5 reactions lie along different paths on the free energy surface. For the k_{-2} step we envision a transition state that contains a slightly dissociated AN and a slightly rearranged acetyl ligand. A more detailed analysis of the electronic and steric profiles of the k_5 step will be reported in the near future.

Acknowledgment. We gratefully acknowledge the donors of the Petroleum Research Fund, administered by the American Chemical Society, for support of this work.

Supplementary Material Available: Computer simulation codes for the square-wave voltammetry and cyclic voltammetry experiments (8 pages). Ordering information is given on any current masthead page.

OM9202130